

A Penta-band Antenna using Symmetrical DGS for RF Energy Harvesting in IoT Applications

Tu Duong Thi Thanh

Faculty of Telecommunication 1, Posts and Telecommunications Institute of Technology, Hanoi, Vietnam
tudtt@ptit.edu.vn

Pham Duy Quan

Faculty of Telecommunication 1, Posts and Telecommunications Institute of Technology, Hanoi, Vietnam
quanpd.b20vt306@stu.ptit.edu.vn

Phan Huu Phuc

Faculty of Telecommunication 1, Posts and Telecommunications Institute of Technology, Hanoi, Vietnam
phucph.b21vt351@stu.ptit.edu.vn

Hoang Thi Phuong Thao

Faculty of Electronics and Telecommunications, Electric Power University, Hanoi, Vietnam
thaohp@epu.edu.vn (corresponding author)

Received: 6 January 2025 | Revised: 6 February 2025 | Accepted: 16 February 2025

Licensed under a CC-BY 4.0 license | Copyright (c) by the authors | DOI: <https://doi.org/10.48084/etasr.10138>

ABSTRACT

The Radiofrequency (RF) energy harvesting technology offers sustainable and non-maintenance power for wireless sensor networks, Internet of Things (IoT) devices, and low-power electronics. Its ongoing advances in improving efficiency are miniaturizing rectennas and making multiple-band antennas capture versatile and efficient electromagnetic radiation across various frequency bands. This paper uses a composed structure of three rings, a symmetrical Defected Ground Structure (DGS), and a shorting pin to construct a penta-band antenna. The antenna operates at 2.4 GHz, 5 GHz, 6 GHz, 7.4 GHz, and 8.7 GHz, with a wide bandwidth of 747 MHz, 286 MHz, 397 MHz, 760 MHz, and 1773 MHz, respectively. Thus, the proposed antenna can capture energy from diverse RF sources such as the IEEE 802.11be standard (WiFi-7), C-band satellite, and radar communications. Furthermore, the proposed antenna achieves a good gain of 2.31 dBi, 4.56 dBi, 4.16 dBi, 5.46 dBi, and 5.41 dBi at resonant frequencies of 2.4, 5, 6, 7.4, and 8.7 GHz, respectively, and a high radiation efficiency of over 90%. Based on the Fire Retardant 4 (FR4) substrate, the eventual size of the antenna is 41.5×37×1.6 mm, which is relatively compact for RF energy harvesting in IoT.

Keywords-penta-band; triple ring; DGS; RF energy harvesting

I. INTRODUCTION

The Internet of Things (IoT) market experiences staggering growth, surpassing USD 100 billion in 2022 [1]. Projections indicate a robust 25.7% Compound Annual Growth Rate (CAGR), catapulting the market to more than USD 784 billion by 2032. This exponential growth underscores the increasing number of IoT devices, particularly sensors and low-power consumer IoT equipment, revolutionizing smart agriculture, intelligent transportation, and industrial monitoring. Radiofrequency (RF) energy harvesting is a cutting-edge green technology. It harnesses ambient electromagnetic energy and

converts it to Direct Current (DC). This DC power source supports low-power electronic devices in IoT systems. The technology's most significant advantage is its ability to provide a continuous and renewable power source for IoT applications, particularly in scenarios where battery replacement is challenging or impractical. Various antennas have recently been proposed for RF energy harvesting [2-21]. Among these, some are single-band antennas designed to achieve high gain [2-8]. However, although these antennas can efficiently extract a single operating frequency, they often result in a relatively compact size with limited bandwidth. Typically, these antennas

target IEEE 802.11 standard (Wi-Fi) frequencies such as the 2.4 GHz band [2-4, 6, 7] and the 5/5.8 GHz band [5, 8]. Other studies have proposed broadband [9-12] or ultra-wideband [13] antennas capable of harnessing various RF sources for DC conversion. Despite their versatility, these antennas often suffer from suboptimal S11 reflection coefficients across all bands, leading to poor impedance matching and, consequently, reduced reception performance. On the other hand, multiband antennas present a more effective solution for RF energy harvesting due to their ability to provide high gain, wide bandwidth, and superior RF-to-DC conversion efficiency [18]. Most multiband antenna studies focus on Wi-Fi bands, specifically 2.4 GHz [14-16, 18, 21] and 5.8 GHz [14, 20, 21].

This study presents a penta-band antenna design composed of a triple ring, a symmetric Defected Ground Structure (DGS), and a shorting pin connecting the above structures to achieve compact size. This antenna operates at 2.4, 5, 6, 7.4, and 8.7 GHz with a wideband of over 5% for five resonant frequencies. Thus, it can leverage Wi-Fi 4/5/6/7, C-band satellite, and radar application waves for RF energy harvesting.

II. ANTENNA DESIGN

A. Draft Calculation

Theoretically, the resonant frequency of an antenna is determined by its physical dimensions. In the case of traditional circular or rectangular microstrip antenna structures, only a single resonant frequency can be defined [22]. To create multiband antennas, this study proposes a novel dual-ring structure that cooperates synergistically to generate the desired resonant frequencies. The antenna design has three parts: the radiation plane, the ground plane, and the shorting pin, as shown in Figure 1.

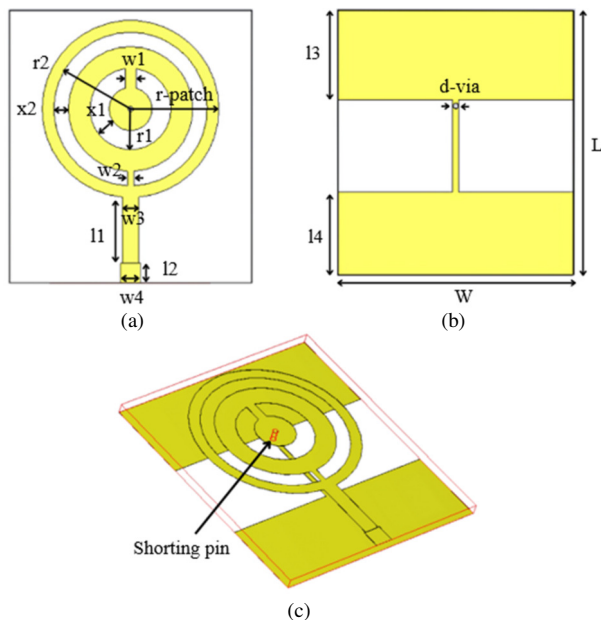


Fig. 1. The structure of the penta-band antenna: (a) Radiation plane, (b) ground plane, (c) 3D structure.

The radiating surface of the antenna comprises a structure of three rings with five distinct radii. This study achieved resonances at the desired five operating bands by calculating five radii of the three-ring elements. The effective radius of each circle, r_i can be calculated by the following formula [22]:

$$f_i = \frac{1.8412c}{2\pi r_i \sqrt{\epsilon_r}} \quad (1)$$

where f_i is the desired resonant frequency.

The principle of making a multiband from the multi-ring structure can be explained based on the equivalent circuit. Figure 2 shows a single-band Microstrip Antenna (MSA) with its equivalent circuit [23], where R and L are resistance and inductance that are formed by the characteristics of the radiation patch, and C is the capacitance formed by both the copper of the patch and the ground. If the slots are etched on the copper of the patch, the electrical length will be lengthened, and more capacitances (c_{slot}) will be generated, as shown in Figure 3. Adding a shorting pin or making DGS are the ways to achieve the multiband antenna.

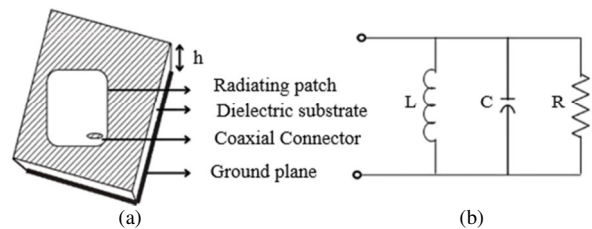


Fig. 2. (a) The traditional patch antenna and (b) its equivalent circuit.

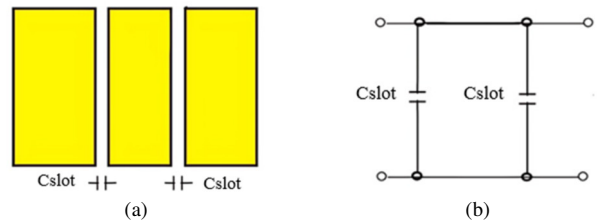


Fig. 3. Slots on the patch antenna: (a) Slots on the patch, (b) the equivalent circuit.

A shorting pin whose height is lengthened on the ground is applied to optimize the antenna's size [24], as shown in Figure 1(c). Under high-frequency conditions ($f > 500$ MHz), the skin deep of a wire is calculated as follows [25]:

$$\delta = (\pi f \mu \sigma_{cond})^{-1/2} \quad (2)$$

where f is the operating frequency, μ is permeability, and σ_{cond} is the conductivity of the copper wire. As the operating frequency increases, the skin depth becomes thinner. This effect may also apply to the copper "via" part of the shorting-pin design in Figure 1. To ensure this effect, the "via" structure was evaluated on a Computer Simulation Technology (CST) simulation with the copper width of the "via" being changed from a thin copper layer to a solid "via". Figure 4 presents the simulation results. It is obvious that the reflection coefficient of the antenna is the same when the copper width of the "via" is increased from 0.035 mm to 0.45 mm. Thus, the "via" shorting

pin was designed with a thin layer of copper, as shown in Figure 1, to make the antenna fabrication much easier.

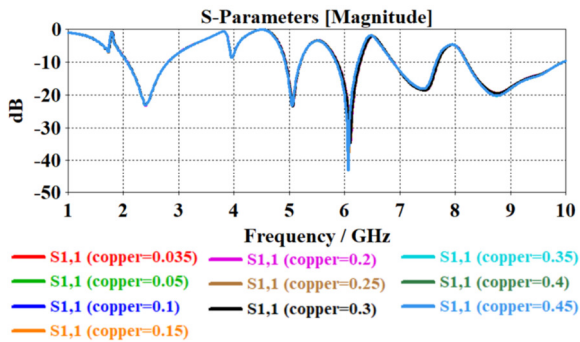


Fig. 4. Making slots on the patch antenna.

B. Optimized Dimensions

To accurately achieve the desired resonant frequencies and wide enough bandwidth to leverage as much as possible the RF energy of these bands, the ring sizes were optimized using the CST software after being draft calculated:

- The patch's radius significantly affects the antenna's resonant frequency. As shown in Figure 5(a), the resonance at all frequencies decreases when the radius increases from 13 to 14 mm with a step of 0.5 mm. This is because increasing the radius extends the antenna's electrical length.
- The width of the first circular cut (x_1) has a significant impact on the 6 GHz band, as illustrated in Figure 5 (b). This parameter can be adjusted to specifically target the aimed resonance while causing only minor alterations in other bands.
- The width of the microstrip line (w_3): In Figure 5 (c), the influence of this line's width shows that if the width increases, the resonance at the lowest frequencies will increase, and the resonance at the highest frequency will significantly decrease.

Table I details the specific dimensions of the proposed antenna. Based on a Fire Retardant 4 (FR4) substrate with a dielectric constant of 4.3 and an $h = 1.6$ mm thickness, the total antenna is 41.5×37 mm², a compact size for RF energy harvesting in portable and IoT equipment.

TABLE I. PROPOSED ANTENNA DIMENSIONS

Parameter	Value (mm)	Parameter	Value (mm)	Parameter	Value (mm)
L	41.5	x_2	2.2	l_2	3
W	37	w_1	1.6	l_3	14
r_{patch}	13.5	w_2	1	l_4	12
r_1	6.2	w_3	2.5	d-via	0.9
r_2	11.7	w_4	3		
x_1	2.9	l_1	10.06		

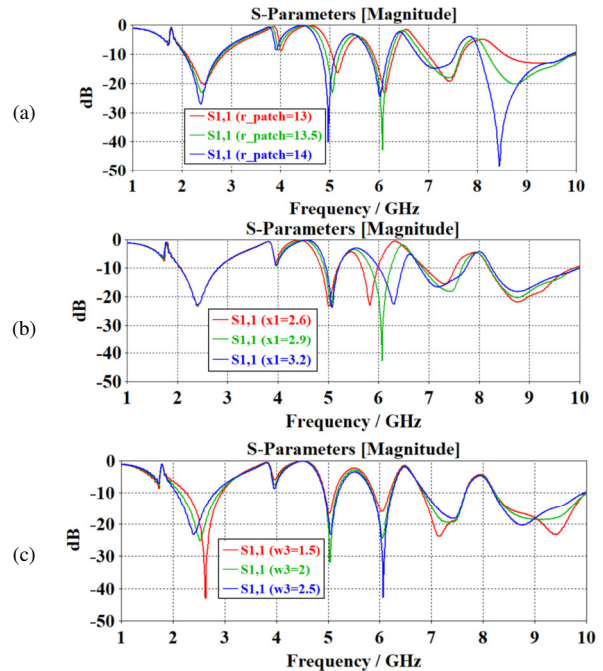


Fig. 5. Analysis of the size parameters affecting the reflection coefficient characteristics: (a) Effect by r_{patch} dimension, (b) Effect by x_2 dimension (c) Effect by w_3 dimension.

III. SIMULATION RESULTS

CST electromagnetic field simulation software was used to analyze and evaluate the antenna characteristics, such as bandwidth, which is determined by the reflection coefficient (S_{11}), resistance matching, which is assessed by the input impedance, directivity, and gain, which are obtained from 2D radiation patterns, and current density at the resonant frequencies.

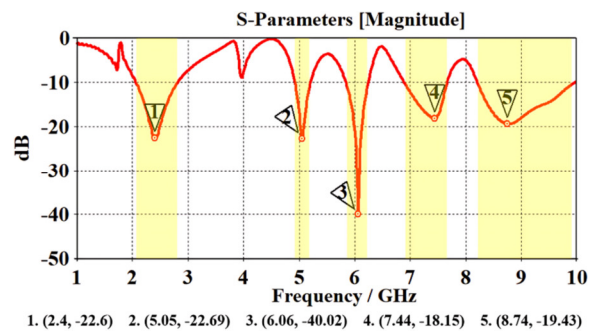


Fig. 6. The antenna reflection coefficient (S_{11}).

Figure 7 shows the penta-band antenna's radiation patterns in 2D mode. The antenna's gains are 2.31, 4.56, 4.16, 5.46, and 5.41 dBi at the resonant frequencies of 2.4, 5, 6, 7.4, and 8.7 GHz, respectively. These values are entirely appropriate for applications involving small-size antennas in terminal devices or IoT sensors.

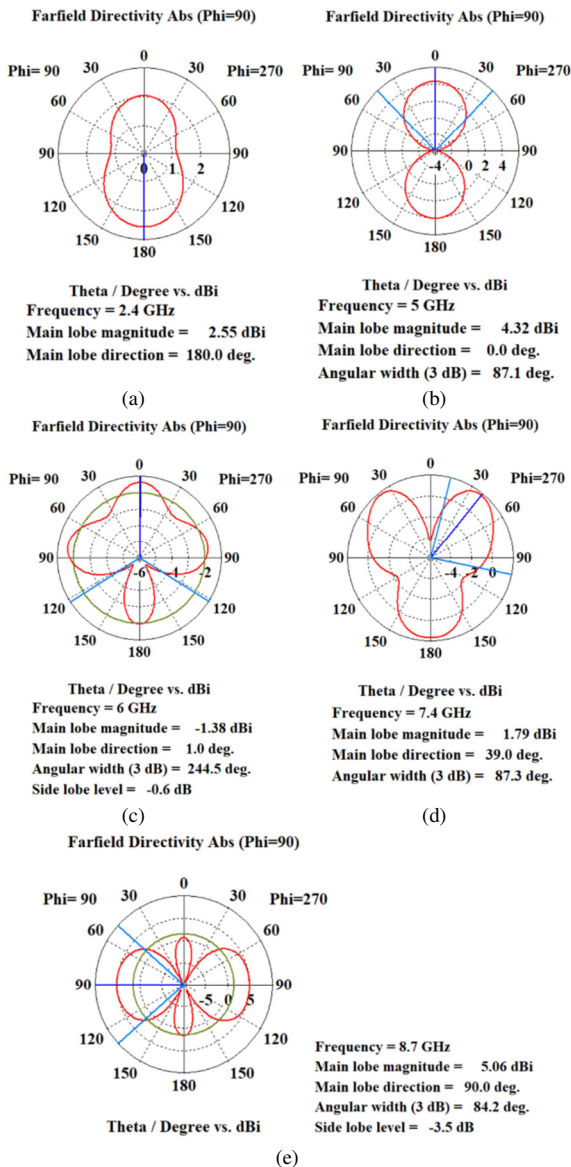


Fig. 7. 2D radiation patterns at different resonant frequencies: (a) 2.4 GHz, (b) 5 GHz, (c) 6 GHz, (d) 7.4 GHz.

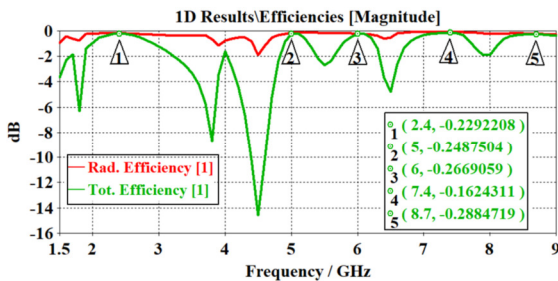


Fig. 8. Efficiency of the proposed antenna.

As shown in Figure 8, the total efficiencies at the resonant frequencies are excellent, all above 90%. Directivities are also 2.51, 5.06, 4.38, 5.55, and 5.66 dBi, respectively. This result is achieved by combining the DGS structure and the shorting pin

extended on the ground plane. This structure has promoted the advantages of the shorting pin in the PIFA antenna, extending the electrical length and improving the radiation efficiency without increasing the antenna size.

To further analyze the effect of the antenna structure on resonant frequencies, the distribution of electric currents was observed on the top plane of the antenna, as shown in Figure 9. It can be noted that the outer ring significantly affects the highest resonant frequency, 8.7 GHz. The 5 GHz band is made by electric current going on two outer rings, while the inner rings focus on the 7.4 GHz band. The electric field focuses mainly on the lengthened shorting pin and DGS to form the 6 GHz band, and the mixing of DGS, shorting pin, and feeding line to make the lowest resonant frequency 2.4 GHz. Based on the difference in the electric field distribution, the proposed antenna can adjust the desired resonant frequency by changing the parameters at the position where the electric field is most concentrated.

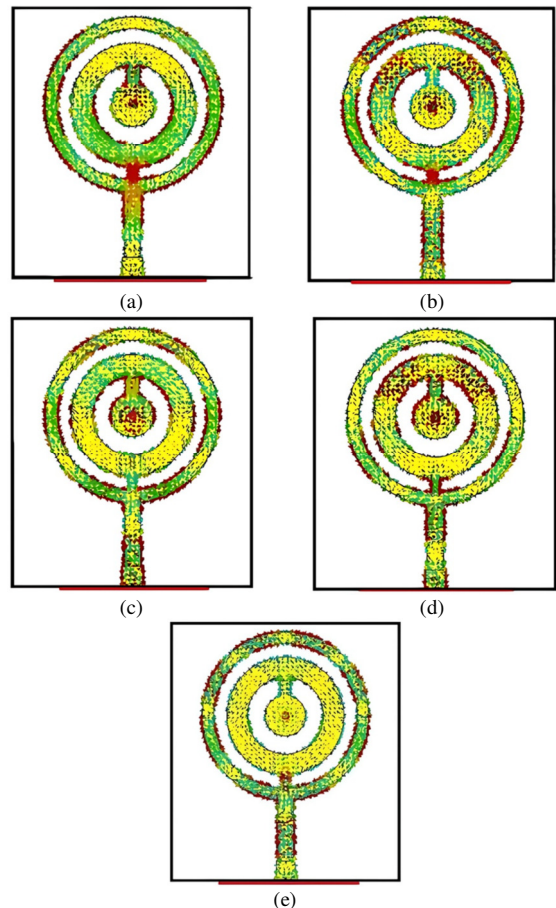


Fig. 9. 2D radiation patterns at different resonant frequencies: (a) 2.4 GHz, (b) 5 GHz, (c) 6 GHz, (d) 7.4 GHz, (e) 8.7 GHz.

The proposed antenna was compared with several previous antenna designs for RF energy harvesting with the same lowest resonance frequency, 2.4 GHz, as seen in Table II. The proposed antenna achieves the five bands with a smaller size and higher efficiency. Furthermore, for applications involving

small-sized antennas for energy harvesting in IoT systems, the gain of the proposed antenna is quite substantial, as it achieves 2.31 dB at a frequency of 2.4 GHz, which is comparable to, if not better than, the dipole antennas used in laptop Wi-Fi transceivers. When comparing these results with previous studies in Table II, it is evident that antennas with higher gain are significantly larger. For instance, the antenna in [2] exhibits a gain 3.4 times higher but is 17 times larger, the antenna in [6] offers a gain 5 times greater but is 142 times larger, and the one in [7] has a gain 3 times higher but is 51 times larger. It is inherent that larger antennas yield higher gains.

TABLE II. COMPARISON OF RECENT 2.4 GHz ANTENNAS

Ref.	Size (mm ³)	f (GHz)	Band No.	B (MHz)	G (dBi)	η (%)
[2]	120×120×3.1	2.45	1	117	7.8	-
[3]	53×59.77×4.5	2.347	1	-	4.8	89
[4]	26.6×23.7×3.2	2.4	1	130	7.2	63
[6]	158×158×14.7	2.45	1	61	11.87	-
[7]	160×80×10.3	2.4	1	137	8.23	-
[14]	67.5×71.5×1	2.45 5.8	2	600 460	-	-
[22]	100×121×1.6	2.4 3.568 4.64 5.87	4	155 146 352 510	3.203 1.519 0.087 2.461	-
This work	41.5×37×1.6	2.4 5 6 7.4 8.7	5	747 286 397 760 1773	2.31 4.56 4.16 5.46 5.41	> 90

IV. MEASUREMENT RESULTS

The triple-ring antenna was fabricated and tested indoors with Vector Network Analyzer (VNA) equipment and outdoors in a wireless system to verify its real performance. Based on the FR4 substrate with a permittivity of 4.3 and a thickness of 1.6 mm, the total size was 41.5×37×1.6 mm³, as shown in Figure 10.

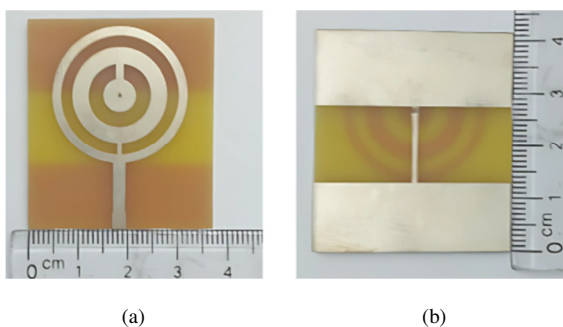


Fig. 10. The fabricated triple-ring antenna: (a) top plane, (b) bottom plane.

A. Indoor Testing

The proposed antenna was tested in the Viettel High Tech (VHT) lab using the VNA ZNB 20 100 kHz-20 GHz, as illustrated in Figure 11. Due to operating on the 2.4/5/6/7.4/8.7 GHz bands, the measured range was chosen from 1 GHz to 10 GHz, covering the antenna's resonant frequencies. The transmit

power level was -10dB to ensure the distance limitation of the lab area. Figure 11 shows that the measured results agree with the simulated. The constructed antenna reaches five operating bands: 2.4, 5, 6, 7, and 8 GHz. The bandwidth assures complete coverage of the working bandwidth of IEEE 802.11ax/be/bd.

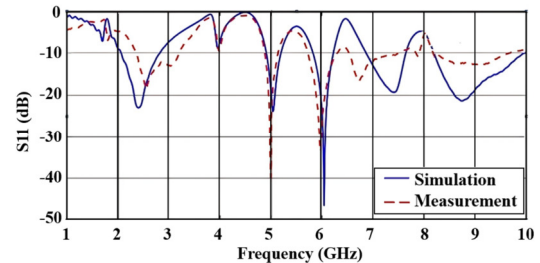


Fig. 11. Comparison of measured and simulated S11 antenna.

B. Outdoor Testing

The performance of the proposed antenna was verified in a natural environment at 2.4 GHz and 5 GHz bands. The test configuration included:

- A D-Link router with two operating bands, 2.4 and 5 GHz, having three antennas with 5 dBi gain.
- A USB Wi-Fi Adapter AC600 for a PC/Laptop, involving a USB 2.0 adapter and a 2.4/5 GHz transceiver.
- The proposed antenna connected to the laptop via a USB AC600 adapter using an SMA transform set.
- The Acrylic Wi-Fi Professional application installed on the laptop.

The performance of the antenna was measured under cloudy weather conditions. The maximum transmission distance achieved between the transmitter and the receiver was 120 m. In this setup, approximately the first 50 m consisted of an open, unobstructed space, allowing for direct line-of-sight communication, while the subsequent 70 m involved a corridor flanked by buildings on either side, introducing potential multipath effects. The multipath effect can result in either signal attenuation or enhancement, depending on the phase variations encountered during wave propagation. This mixed environment effectively simulates realistic conditions to evaluate antenna performance in urban IoT applications. This procedure evaluated two parameters: the Received Signal Strength Indicator (RSSI) and the Signal-to-Noise Ratio (SNR). Figure 14 shows the actual measurements of the proposed antenna in terms of RSSI, which is the same for both the 2.4 and 5 GHz bands. At 120 m, the RSSI was still good, approximately 70 dBm, indicating enough signal strength for packet delivery and leveraging Wi-Fi 4/5/6/7 waves for RF energy harvesting. Figure 15 shows the SNR value of the proposed triple-ring antenna at 2.4 and 5 GHz. It can be observed that the proposed antenna achieves an excellent SNR of more than 60 in both bands for a distance of 120 m [26]. The RSSI and SNR values for a Wi-Fi router typically decrease as the distance from the router increases due to signal attenuation and interference.

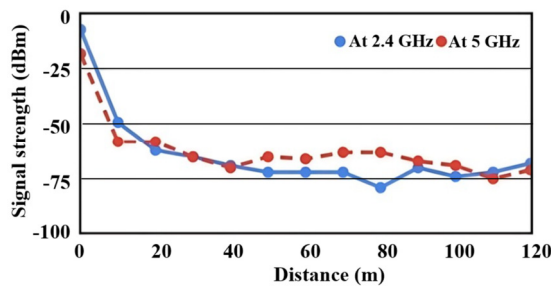


Fig. 12. RSSI measurement.

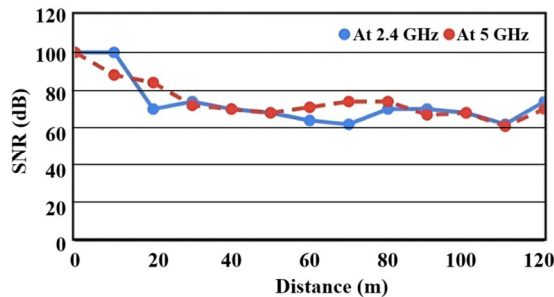


Fig. 13. SNR measurement.

However, the observation that RSSI and SNR values of a Wi-Fi signal do not decrease with increasing distance, particularly within the 40-120 m range, could be explained by the phenomenon of signal resonance due to reflections from buildings on either side of the street as the antenna moves. These reflected signals can constructively interfere with the direct line-of-sight signal, leading to areas where the signal strength remains consistent or even appears to be enhanced. This constructive interference effectively mitigates the typical signal degradation expected with increasing distance, resulting in more stable RSSI and SNR values over the specified range.

V. CONCLUSION

This paper presents a penta-band circular ring antenna using a DGS structure and a shorting pin whose length is lengthened in the ground plane to make a multiband antenna with a decreased size. Operating at 2.4, 5, 6, 7.4, and 8.7 GHz with good efficiency and wide bandwidth, the proposed antenna can leverage Wi-Fi 4/5/6/7, C-band satellite, and radar application waves for RF energy harvesting. Furthermore, based on the analysis of the S11 parameters and the electric field distribution region, this study found that some parameters significantly influence the resonant frequencies. This analysis will help researchers optimize multiband antennas with desired resonant frequencies for diverse wireless applications.

REFERENCES

- [1] "Internet of Things (IoT) Market Size, Share, Growth Analysis," *Market Research Future*. <https://www.marketresearchfuture.com/reports/internet-of-things-market-1176>.
- [2] S. S. Prabhu, C. Tharini, and M. N. M. Aslam, "Design and Performance Analysis of WiFi Microstrip Patch Antenna under Different Bending Conditions using Flexible Substrates," *Engineering, Technology & Applied Science Research*, vol. 14, no. 5, pp. 16790–16796, Oct. 2024, <https://doi.org/10.48084/etasr.8376>.
- [3] X. Liu, M. Li, X. Chen, Y. Zhao, L. Xiao, and Y. Zhang, "A Compact RF Energy Harvesting Wireless Sensor Node with an Energy Intensity Adaptive Management Algorithm," *Sensors*, vol. 23, no. 20, Jan. 2023, Art. no. 8641, <https://doi.org/10.3390/s23208641>.
- [4] M. Wagih, G. S. Hilton, A. S. Weddell, and S. Beeby, "Dual-Band Dual-Mode Textile Antenna/Rectenna for Simultaneous Wireless Information and Power Transfer (SWIPT)," *IEEE Transactions on Antennas and Propagation*, vol. 69, no. 10, pp. 6322–6332, Jul. 2021, <https://doi.org/10.1109/TAP.2021.3070230>.
- [5] X. Cai, W. Geyi, and Y. Guo, "A Compact Rectenna With Flat-Top Angular Coverage for RF Energy Harvesting," *IEEE Antennas and Wireless Propagation Letters*, vol. 20, no. 7, pp. 1307–1311, Jul. 2021, <https://doi.org/10.1109/LAWP.2021.3078548>.
- [6] W. Lee, S. Choi, H. Kim, S. Hwang, S. Jeon, and Y.-K. Yoon, "Metamaterial-Integrated High-Gain Rectenna for RF Sensing and Energy Harvesting Applications," *Sensors*, vol. 21, no. 19, Jan. 2021, Art. no. 6580, <https://doi.org/10.3390/s21196580>.
- [7] I. Mujahidin and A. Kitagawa, "CP Antenna with 2×4 Hybrid Coupler for Wireless Sensing and Hybrid RF Solar Energy Harvesting," *Sensors*, vol. 21, no. 22, Jan. 2021, Art. no. 7721, <https://doi.org/10.3390/s21227721>.
- [8] S. Douhi, T. Islam, R. A. Saravanan, A. Eddiai, S. Das, and O. Cherkaoui, "Design of a Flexible Rectangular Antenna Array with High Gain for RF Energy Harvesting and Wearable Devices.," *Journal of Nano- & Electronic Physics*, vol. 15, no. 3, 2023.
- [9] J. Porras, A. Acosta, A. Corona, and G. Puerto, "Energy harvesting system using broadband textile antennas," *Journal of Applied Research and Technology*, vol. 22, no. 1, pp. 9–21, Feb. 2024, <https://doi.org/10.22201/icat.24486736e.2024.22.1.1979>.
- [10] B. Behera, S. Mishra, M. H. Alsharif, P. Uthansakul, and M. Uthansakul, "A metasurface-inspired printed monopole antenna for 5G and RF energy harvesting application," *Engineering Science and Technology, an International Journal*, vol. 51, Mar. 2024, Art. no. 101638, <https://doi.org/10.1016/j.jestech.2024.101638>.
- [11] Y. Wang *et al.*, "Efficiency Enhanced Seven-Band Omnidirectional Rectenna for RF Energy Harvesting," *IEEE Transactions on Antennas and Propagation*, vol. 70, no. 9, pp. 8473–8484, Sep. 2022, <https://doi.org/10.1109/TAP.2022.3177492>.
- [12] H. Q. Nguyen and M. T. Le, "Multiband Ambient RF Energy Harvester with High Gain Wideband Circularly Polarized Antenna toward Self-Powered Wireless Sensors," *Sensors*, vol. 21, no. 21, Jan. 2021, Art. no. 7411, <https://doi.org/10.3390/s21217411>.
- [13] S. Douhi, G. R. K. Prasad, A. Eddiai, O. Cherkaoui, M. Mazroui, and S. Das, "A Miniaturized Wearable Textile UWB Monopole Antenna for RF Energy Harvesting," *Journal of Nano- and Electronic Physics*, vol. 15, no. 1, 2023.
- [14] L. Li, R. Xu, J. Cao, X. Li, and J. Nan, "A Compact Loop-shaped Dual-band Omnidirectional Rectenna for RF Energy Harvesting," *Progress In Electromagnetics Research M*, vol. 125, pp. 1–9, 2024, <https://doi.org/10.2528/PIERM24010703>.
- [15] R. Maher, A. Allam, H. Kanaya, and A. B. Abdelrahman, "Dualband rectenna for RF energy harvesting using metamaterial reflect array and novel matching technique," *AEU - International Journal of Electronics and Communications*, vol. 173, Jan. 2024, Art. no. 155020, <https://doi.org/10.1016/j.aeue.2023.155020>.
- [16] S. Roy, J. J. Tiang, M. B. Roslee, M. T. Ahmed, A. Z. Kouzani, and M. A. P. Mahmud, "Quad-Band Rectenna for Ambient Radio Frequency (RF) Energy Harvesting," *Sensors*, vol. 21, no. 23, Jan. 2021, Art. no. 7838, <https://doi.org/10.3390/s21237838>.
- [17] S. Muhammad, J. J. Tiang, S. K. Wong, A. Smida, R. Ghayoula, and A. Iqbal, "A Dual-Band Ambient Energy Harvesting Rectenna Design for Wireless Power Communications," *IEEE Access*, vol. 9, pp. 99944–99953, 2021, <https://doi.org/10.1109/ACCESS.2021.3096834>.
- [18] S. Roy, R. J. J. Tiang, M. B. Roslee, Md. T. Ahmed, and M. A. P. Mahmud, "Quad-Band Multipoint Rectenna for RF Energy Harvesting in Ambient Environment," *IEEE Access*, vol. 9, pp. 77464–77481, 2021, <https://doi.org/10.1109/ACCESS.2021.3082914>.

- [19] A. D. Boursianis *et al.*, "Triple-Band Single-Layer Rectenna for Outdoor RF Energy Harvesting Applications," *Sensors*, vol. 21, no. 10, Jan. 2021, Art. no. 3460, <https://doi.org/10.3390/s21103460>.
- [20] P. Zhang, H. Yi, H. Liu, H. Yang, G. Zhou, and L. Li, "Back-to-Back Microstrip Antenna Design for Broadband Wide-Angle RF Energy Harvesting and Dedicated Wireless Power Transfer," *IEEE Access*, vol. 8, pp. 126868–126875, 2020, <https://doi.org/10.1109/ACCESS.2020.3008551>.
- [21] M. M. Hasan and A. M. Sabaawi, "A modified fractal hexagonal slot antenna with a defected ground structure for RF energy harvesting applications," *International Journal of Microwave and Optical Technology*, vol. 19, no. 2, pp. 169–170, Mar. 2024.
- [22] C. A. Balanis, *Antenna Theory: Analysis and Design*. John Wiley & Sons, 2015.
- [23] A. Singh *et al.*, "A Review: Circuit Theory of Microstrip Antennas for Dual-, Multi-, and Ultra-Widebands," in *Modulation in Electronics and Telecommunications*, IntechOpen, 2020.
- [24] T. T. T. Duong, V. Y. Vu, T. N. Nguyen, N. T. Nguyen, H. D. Nguyen, and T. T. To, "4x4 Dual-band MIMO antenna with low mutual coupling using a novel structure of neutral line," in *2017 International Conference on Advanced Technologies for Communications (ATC)*, Quy Nhon, Vietnam, Oct. 2017, pp. 80–85, <https://doi.org/10.1109/ATC.2017.8167647>.
- [25] R. Ludwig and G. Bogdanov, *RF Circuit Design: Theory and Applications*. Prentice Hall, 2000.
- [26] A. Vlavianos, L. K. Law, I. Broustis, S. V. Krishnamurthy, and M. Faloutsos, "Assessing link quality in IEEE 802.11 Wireless Networks: Which is the right metric?," in *2008 IEEE 19th International Symposium on Personal, Indoor and Mobile Radio Communications*, Cannes, France, Sep. 2008, pp. 1–6, <https://doi.org/10.1109/PIMRC.2008.4699837>.